# Modeling effects of common molecular contaminants on the Euclid infrared detectors

W. Holmes, C. McKenney, R. Barbier, H. Cho, A. Cillis, et al.

**SPIE.**

# Modelling Effects of Common Molecular Contaminants on the Euclid Infrared Detectors

W. Holmes[a], C. McKenney[a,b], R. Barbier[j], H. Cho[a], A. Cillis[c], J-C. Clemens[d], O. Dawson[a], G.Delo[e], A. Ealet[d], A. Feizi[f], N. Ferraro[a], R. Foltz[g], T. Goodsall[a], M. Hickey[g], T. Hwang[h], U Israellson[a], M. Jhabvala[g], D. Kahle[g], Em. Kan[g], Er. Kan[g], G. Lotkin[g], T. Maciaszek[l], S. McClure[a], L. Miko[g], L. Nguyen[c], S. Pravdo[a], E. Prieto[k], T. Powers[c], M. Seiffert[a], P. Strada[i], C. Tucker[c], K. Turck[e], A. Waczynski[g], F. Wang[h], C. Weber[a], and J. Williams[e]

[a]Jet Propulsion Laboratory, Pasadena, California, 91109 USA
[b]National Institute of Standards and Technology, Boulder, CO, USA
[c]University of Maryland Baltimore County, Baltimore, MD USA 21250 USA
[d]CNRS, Centre de Physique des Particules de Marseille, 163 Ave. de Luminy, Marseille 13009 FR
[e]Global Science and Technology, 7855 Walker Drive, Greenbelt, MD 20770 USA
[f]AK Aerospace Technology Corporation, 4300 B St., Anchorage, AK 99503 USA
[g]NASA Goddard Space Flight Center, Greenbelt, Maryland 20771 USA
[h]Arctic Slope Regional Corporation, 7000 Muirkirk Meadows Dr., Beltsville, MD 20705 USA
[i]European Space Research and Technology Centre, Keplerlaan 1, AZ Noordwijk 2201 NL
[j]Institut de Physique Nucleaire de Lyon, 4, rue Enrico Fermi, Lyon, France
[k]Laboratoire d Astrophysique de Marseilles, Site de Chauteau-Gombert 38, rue Frederic Joilot-Curie, Marseille, France
[l]CNES, Centre National dEtudes Spatiales, 31401 Toulouse, France

## ABSTRACT

Cleanliness specifications for infrared detector arrays are usually so stringent that effects are neglibile. However, the specifications determine only the level of particulates and areal density of molecular layer on the surface, but the chemical composition of these contaminants are not specified. Here, we use a model to assess the impact on system quantum efficiency from possible contaminants that could accidentally transfer or cryopump to the detector during instrument or spacecraft testing and on orbit operation. Contaminant layers thin enough to meet typical specifications, $< 0.5 \mu gram/cm^2$, have a negligible effect on the net quantum efficiency of the detector, provided that the contaminant does not react with the detector surface, Performance impacts from these contaminant plating onto the surface become important for thicknesses $5 - 50 \mu gram/cm^2$. Importantly, detectable change in the "ripple" of the anti reflection coating occurs at these coverages and can enhance the system quantum efficiency. This is a factor 10 less coverage for which loss from molecular absorption lines is important. Thus, should contamination be suspected during instrument test or flight, detailed modelling of the layer on the detector and response to very well known calibrations sources would be useful to determine the impact on detector performance.

**Keywords:** Euclid, mercury cadmium telluride detectors, infrared focal planes, IR detector arrays, contamination

Further author information: (Send correspondence to W.H.)
W.H..: E-mail: warren.a.holmes@jpl.nasa.gov, Telephone: 1 818 354 5049

# 1. INTRODUCTION

The prime objective of EUCLID is to study the geometry and the nature of the dark Universe (dark matter, dark energy) with unprecedented accuracy.[1, 2] This mission will investigate the distance-redshift relationship and the evolution of cosmic structures by measuring shapes and redshifts of distant galaxies out to redshifts 2, or equivalently by looking back 10 billion years of cosmic history. It combines several techniques of investigations, also called cosmological probes, in a very large survey over the full extragalactic sky. Among those cosmological probes, two of them play a major role in the EUCLID mission concept and the instrumental approach: the Weak Gravitational Lensing (WL) and the Baryon Acoustic Oscillation (BAO).

The mission baseline is for EUCLID to be launched by a SOYOUZ ST 2-1B from French Guyana Space Center before the end of 2020. The EUCLID Spacecraft will be placed into an orbit around the Earth-Sun langrange point, L2. The EUCLID nominal in-orbit operation phase includes commissioning and scientific operations for 7 years. Two instruments are part of the primary Korsch telescope. They are the Visible Imager (VIS)[3] and the Near Infrared Spectro-Photometer (NISP).[4] The focal plane of NISP consists of 16 infrared focal plane arrays cooled to 100K, each with dedicated cryogenic readout electronics cooled to $\sim 135K$. The cooling for each is provided by passive radiators on the Euclid spacecraft. NASA is providing and testing the focal plane arrays, cryogenic flex cables and control electronics for NISP. The focal plane array and cryogenic electronics are the $HgCd_xTe_{1-x}$ photodiode arrays with the HAWAII 2 RG Read Out Integrated Circuit (ROIC) and SIDECAR ASIC[5] developed and manufactured by Teledyne Imaging Systems.

A key specification for these components is a maximum particulate and moelcular contamination. The specifications are driven to maintain optics cleanliness to maintain high end to end optical efficiency and low stray light levels. The direct impact on the detector is not commonly a concern nor analyzed. The detector is designed to absorb all incident photons so small changes in loss are perhaps not viewed as important. Also it is the transmittance of the photons through the contaminant important for detector performance, whereas for optics scattering and absorptive loss are more significant. Furthermore, once integrated into the instrument and spacecraft, the detectors are usually maintained at a temperature lower than the optics. Thus water, air and organics can preferentially condense on the detector surfaces. Effects of condensation of outgassing during testing and flight, from MLI for example, has been observed on GAIA[6] and OCO-II.[7] Here we develop a model of clean detector surface and compute the change in net QE due to a single uniform layer of molecular contaminant as a function of contaminant thickness. Contaminants used for analysis are water ice, carbon dioxide ice, and silicone, all of which are inert on the detector surface. Our modelling of the effects on detector performance shows the following. Contaminants meeting molecular specifications $< 0.5 \mu grams/cm^2$ or $< 5nm$ thick have negligible impact on net QE or detector system optical efficiency . Contaminant thicknesses in the range $50 - 250nm$, cause a modulation of the " clean " anti reflection (AR) coating but without absorptive loss. Only for films exceeding several $\mu m$ in thickness do infrared absorption lines become apparent at a significant level in optical efficiency. This work suggests further studies of non-uniformity in contaminant films to quantify margin to cleanliness requirements and to identify tell tale spatial patterns in flat field response that indicate contaminant films are present or changing during observation campaigns.

# 2. ANTIREFLECTION COATING MODEL AND ASSUMPTIONS

To establish the baseline net QE for a clean detector, we use measurements of absolute QE on prototype H2RG for Euclid taken at the Detector Characterization Laboratory at Goddard Space Flight Center. QE data are sampled using a monochromoter at 50nm resolution over the range $0.7 - 2.55 \mu m$. The absolute QE is obtained from cross calibration with a NIST traceable, calibrated reference diode. Bin to bin precision is estimated to be $< 1\%$ and absolute accuracy is estamted to be $< 5\%$. The design of the anti-reflection (AR) coating used on these detectors is proprietary. So here we discuss generic antireflection coating matching conditions that would enable the simplest function model to be fit to measured QE values. Any AR coating depends first on the index of referation of the base layer, which is the $HgCd_xTe_{1-x}$ detector material. For Euclid, the material is grown to have a 2.3$\mu m$ cutoff. This has fractional composition $x = 0.484$ for the $HgCd_xTe_{1-x}$ which has a $n_{HgCd_xTe_{1-x}} \approx 3.0$ at the $100K$ operating temperature.[8]

The simplest anitreflection coating is the quarter-wave coating which adds an appropriate phase shift and impedance matching to the incident radiation such that it can travel from the initial medium (typically vacuum,

$n = 1$) to the final material ($n_f$). When looking at the final load through an effective quarter-wave coating the load impedance is transformed to

$$Z_{in} = \left(\frac{Z_0}{n_1}\right)^2 \times \left(\frac{n_f}{Z_0}\right) = Z_0 \frac{n_f}{n_1} \tag{1}$$

where $Z_0 \approx 377\ \Omega$ is the impedance of free space. To minimize reflected power the input impedance should match the impedance of free space, $Z_{in} = Z_0$ which imposes the condition for the AR coating layer

$$n_1 = \sqrt{n_f} \tag{2}$$

The expected absorbed-power for an ideal single layer AR coating with a center wavelength of 1200 nm is shown in Figure 1.

A double layer allows a larger bandwidth coating to be made. In this configuration the input impedance looking in to the first layer (assuming two quarter wave layers) is

$$Z_{in} = Z_0 \left(\frac{n_2}{n_1}\right)^2 \frac{1}{n_3} \tag{3}$$

And the ideal condition is that the ratio between the indices of refraction is

$$n_1 = \frac{n_2}{\sqrt{n_f}} \tag{4}$$

Ideal single and double layer AR coatings are shown in Figure 1. The double layer AR coating shows significantly more bandwidth than the ideal single layer coating. This bandwidth of this ideal double layer AR coating is on par with the bandwidth in the detectors. So we use a two layer model to fit the data. The AR coating model is computed from first principles boundary conditions for electric and magnetic fields and applied to multiple layers using an S matrix formalism and fit to the QE data over the band, $0.9 - 2.2\mu m$ relevant to detectors in the NISP focal plane.

For the model AR coating, we use a ZnS layer, since this material has been used often in $HgCd_xTe_{1-x}$ detectors.[8] For the model, the wavelength dependent refractive index at 100K is used.[9, 10] For the top layer in our model we fit the measured data with one of two standard passivation layers, $SiO_2$ and $Al_2O_3$. The data fit with $Al_2O_3$, with $n_{Al_2O_3} \approx 1.65$ constant over the band, were better. So the AR coating in our model of a clean detector is a $Al_2O_3$ on ZnS on $HgCd_xTe_{1-x}$.
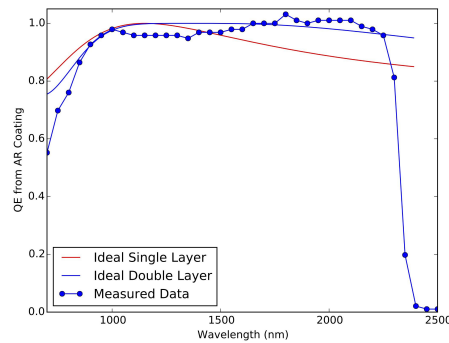


Figure 1. Quantum Efficiency (QE) of the simple AR models with ideal materials. For the single layer, $n_1 = 1.73(\approx \sqrt{3.0})$ while in the two-layer model $n_1 = 1.33$ and $n_2 = 2.3$. Terminal load is $HgCd_xTe_{1-x}$ with $n = 3.0$. Real data is overlaid to qualitatively compare the measured bandwidth with these two models.

Effects of lower quality films impacts the fits only at the shortest end of the band and is not included in the model. The $HgCd_xTe_{1-x}$ material cutoff at $2.3\mu m$ is outside the fit range. The results of the model AR coating fits to measured QE for prototype deectors is shown in Figure 2. The fit includes an overall multiplier to account for the detection efficiency in the $HgCd_xTe_{1-x}$ layer and calibration accuracy of the measurement.
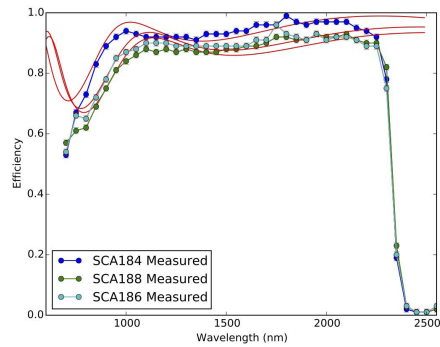
Figure 2. Fitting Datal To Model. Red line is the fit described above. Error bars are the 1% error bars used in the measurement setup, while an overall 5% multiplier is applied to a simple fitting model of a ZnS / Al2O3 AR coating. The rolloff around 2.3 $\mu$m is likely due to the content of the $HgCd_xTe_{1-x}$ and allows an approximate $x \approx 0.5$ to be determined to account for detector performance. The low-wavelength roll off is likely not due to the AR structure but may be some other filtering in the system and the low-wavelength cut-off of ZnS, which generally varies between 350 and 600 nm depending on the details of sample preparation.

## 3. CONTAMINATION

Contamination requirements are quoted in terms of the standardized specification.[11] For example 250-A/2, specifies cleanliness as following. The cleanliness level, $L = 250$, sets a maximum of only one particle of size $250\mu m$ can be found over an area of $0.1m^2$, and no larger sized particle. Smaller sized particles, of linear dimension $x$, follow a log normal distribution,[11] shown in Equation 5,

$$\log(N) = 0.926 \left( \log^2(L) - \log^2(x) \right).$$ (5)

The second symbol specifies molecular contamination. For A/2, no more than $1/2\mu gram/cm^2$ is present over the same $0.1m^2$. The chemical constitutents are not specified. If one assumes that the particulate density is $1g/cc$, the particulate and moelcular contamination levels are self consistent.

Prior to integration, particulate contamination is controlled by cleanroom practice. Routine microscopic inspections are also performed so that mciron dimension particles can be found and removed,. Molecular con-taminiation can occur at various points during integration, test and space flight operations and can possibly go undetected until after launch. The effect of molecular contamination, specifically for materials listed in Table 1, is the focus of this modelling effort. The most pervasive contaminant is water since it can be trapped on many surfaces at ambient temperature and then outgas later. If significant amounts of air are trapped in the instru-ment or test chamber during cool down, $CO_2$ in the trapped air could freeze out onto the detectors. Both water and $CO_2$ contamination could occur both in ground test of the instrument and after launch. Contaminants that could possibly be introduced during ground testing include silicone pump oil and other organic oils. Silicone pump oil is the most tenacious, even when instrument components and the test chamber are precision cleaned. In practice, once a component contaminated with silicone oil is introduced to an environment, it migrates to all components. In all of these cases, it is either very expensive to de-integrate and clean the detectors, or impossible once it is in space. Thus the goal of the modelling is to determine lower limits on contamination that produce, first, a noticable effect and, second, an adverse effect on detector performance.

We assume the contaminant is a smooth layer on top of the AR coating, so it acts as another layer in the AR coating stack. The measured real and imaginary components are used for water ice[12] and $CO_2$ ice[13] shown in Figure 3. Silicone is general class of complex molecules with low viscosity (oil) to high viscosity (grease). We use properties of a standard low vapor pressure pump oil; silicone 704 or 1,1,5,5-Tetraphenyl-1,3,3,5-tetramethyltrisiloxane for our analysis.[14] For this silicone oil, detailed measurements of refractive index

Table 1. Material properties of selected contaminants.

| Contaminant | Melting T | Density | Band Average $Re(n)$ | A/2 Thickness |
|---|---|---|---|---|
| | K | g/cc | | nm |
| Water Ice $I_h$ | 273 | 0.93 | 1.29 | 5.4 |
| $CO_2$ | 194 | 1.6 | 1.40 | 3.1 |
| Silicone oil | | 1.07 | 1.55 | 4.7 |

over the visible to near infrared range are not readily available. The real part of the index is weakly dependent on wavelength in the visible an near infrared. To model the effect of silicone on the AR coating, we use only a constant real index of refraction in Table 1. Measured transmittance on a silicone sample 2 millimeters thick shows absorption bands from 1-2 $\mu m$.[15] Although more complicated a molecule than water, the general broadness of absorption bands are similar to water, but the absorption coefficient is smaller than water. So thickness where absorption is significant are greater than that of water.
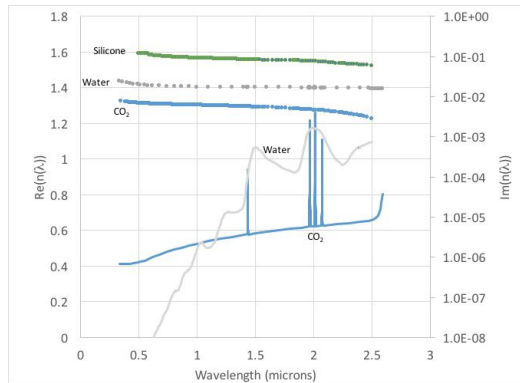


Figure 3. Real (left y-axis) and imaginary (right y-axis) refractive for water ice and $CO_2$ ice as a function of wavelength in the visible and near infrared. The real component is plotted on a linear-linear scale, the imaginary component is plotted on a log-linear scale.

Starting with the model AR coating. the net QE is computed for various thicknesses of the contaminant as a third layer of the AR coating. The lowest thickness corresponds to A/2 as listed in Table 1 and shown in Figure 4. At thicknesses in the range 50-250nm, the shape of the net QE changes from that of the AR coating for the clean surface as shown in Figure 5, 6 and 7. At these thicknesses the absorption features are $\sim 0.1\%$ and smaller than the changes in net QE ripple. Only for thicknesses $> 1\mu m$, shown in Figure 8, is the contaminant thick enough that absorption lines are significant compared to the ripple. An alternative way to assess the effect of contamination is to compute the average QE over a given band. Here we average over the band $0.9 - 2\mu m$. For the A/2 thickness cases the contaminated surface QE is $0.1 - 0.2\%$ lower than the clean surface. However, for contaminant thickess of 250nm, the average QE *increases* by $1 - 3\%$ compared to the clean surface! When the loss is important, thicknesses $> 1\mu m$, the QE decreases by many percent. For Euclid, this would manifest as a change in color correction in each of the 3 photometry bands when comparing measurements from reference sources in the calibration fields.

## 4. DISCUSSION

At the A/2 level, the effects of molecular contamination are negligible within the accuracy of the measurements $\sim 1\%$, confirming the intent of the stringent requirement on cleanliness. Even if the A/2 standard of cleanliness is achieved for the instrument, payload (telescope) and test chambers, aluminized mylar multilayer insulation (MLI) included for thermal insulation can outgas during operation and reconvene on the cold detector surface. Thus it
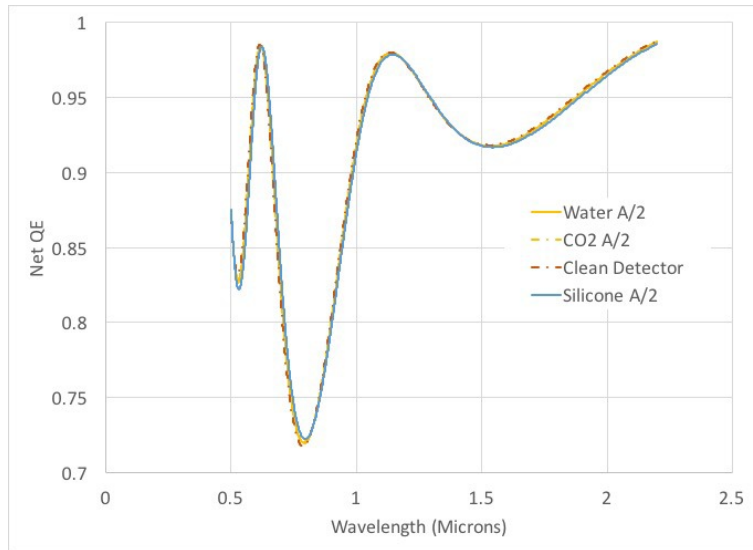
Figure 4. Net QE as a function of wavelngth for a clean detector and A/2 coverage for water ice, $CO_2$ ice and silicon. Effects are $< 0.1\%$ over the entire Euclid band 1-2 $\mu m$. An effect is noticable at the 0.1% level near $0.5\mu m$.
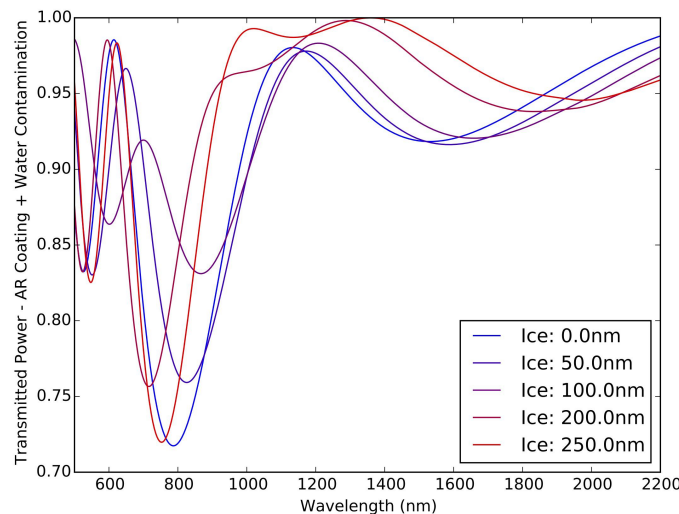


Figure 5. Net QE as a function of wavelngth for several thicknesses of water ice.

is possible for the water or other residue to accumulate on the focal plane giving an approximate thickness of 6 nm, about 10 monolayers, multiplied by the relative difference in surface areas. The spacecraft and instrument payload are complicated re-entrant structures at different temperatures that range from $300 - 85K$. The area of the external shell is $\sim 60m^2$;[16] if $\sim 100$ layers of MLI are used, the total surface area in the space craft is of order $6000m^2$. The surface area of the NISP focal plane mosaic is $0.02m^2$ or between 3ppm (w/ MLI) to 300ppm (no MLI) of the total surface area. Less than 0.1% of the total water need migrate to the focal plane structure to create a 50nm layer on the detector, which, as shown in the previous section, produces a measureable change in the net QE. As found in even recent space science missions, it is critical to ensure there are no significant trapped volumes and that MLI is in an open environment so that water and other gases are evacuated to space before condensing on important instrument surfaces, including the detector.

$CO_2$ which is non polar does not adhere to spacecraft surfaces and MLI as well as water. So the main source of $CO_2$ are from leaks in test chamber leaks during ground test campaigns and from air trapped in spacecraft
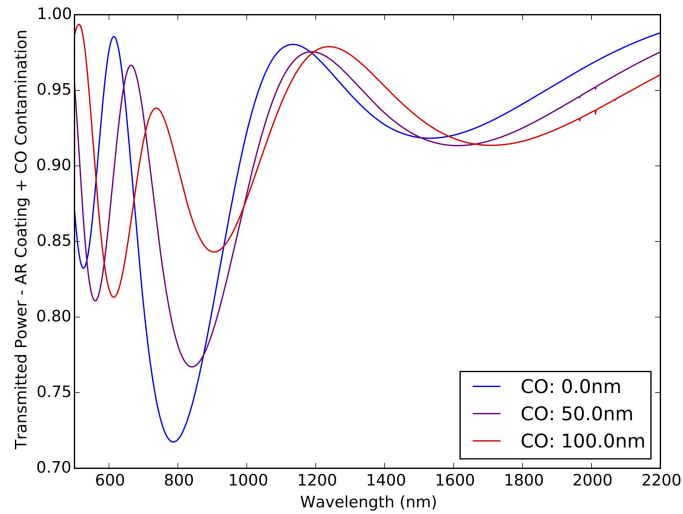
Figure 6. Net QE as a function of wavelngth for several thicknesses of $CO_2$ ice.
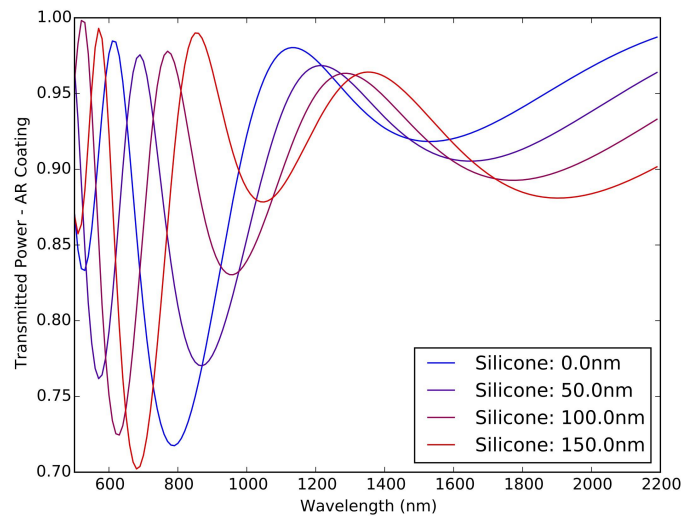


Figure 7. Net QE as a function of wavelngth for several thicknesses of silicone on detector surface.

while the detectors (and focal plane array) cool to 100K. An accumuation of A/2 and 100nm thick later of $CO_2$ are $\sim 0.4$ and 13 mg on the focal plane. At a "bad" leak rate of $10^{-2}scc/sec$, into the test chamber, it would take years to accumulate this amount of $CO_2$ on the detectors. The air within the spacecraft volume, $\sim 34m^3$, while it is on the launch pad is a source of $\sim 20$grams of $CO_2$. The spacecraft within the fairing has very little flow impedance to the environment thus is in steady state with the ambient atmosphere on ascent. So once reaching low earth orbit, less than a picogram of $CO_2$ remains in the open volume of the spacecraft, making $CO_2$ a very unlikely contaminant. Finally, silicone migrating in the instrument system has been shown to have an effect first on the ripple in the AR coating. Thus effects of silicone contamination appear to be being and in fact might be missed. Only films many microns thick present a problem for the detector. However, this films is so thick, it would not occur given standard clean room practices.
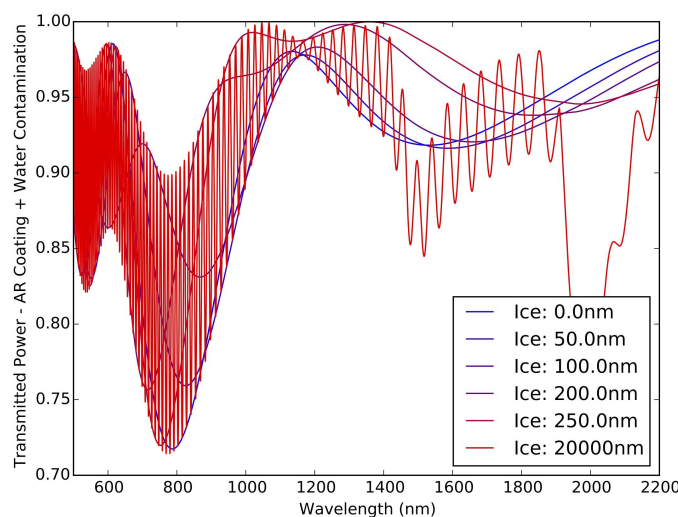
Figure 8. Net QE as a function of wavelength with a $2\mu m$ thick layer of water ice. At this thickness ripple and absoprtion features are comparable in size.

## 5. CONCLUSIONS

We have modeled the effect of uniform films of molecular contaminants on infrared detector surface. At an A/2 coverage, water, $CO_2$ and silicone oil have neglible effect to the detector optical efficiency in the NISP band $\sim 0.9 - 2\mu m$. For contaminant films $\sim 50 - 250nm$ thick, the ripple in the AR coating changes by several percent as compared to that with a clean detector surface. At some coverages, water, $CO_2$ or silicone oil even enhance the net QE by a few percent. Signatures due to the absorption begin to affect the net QE at coverages > several $\mu m$. Importantly, significant modulation of the net QE occurs at coverages 10-100 times thinner than when a problem can be identified by a molecular absorption lines of $CO_2$ or broadband loss from water or silicone. Thus should contamination be suspected during ground test or flight, modelling of the layer as an additional AR coating layer on the detector should be performed. This would allow estimates in the change of color corrections to be assessed. Other studies of non-uniformity in contaminant films could prove useful to further quantify margin to cleanliness requirements as well as catalog tell-tale spatial patterns in flat field response.

## ACKNOWLEDGMENTS

## REFERENCES

[1] Laureijs, R. et al., "Euclid deinition study report," *arXiv:1110.3193 [astro-ph.CO]* (2011).

[2] Laureijs, R. et al., "Euclid: ESAs mission to map the geometry of the dark universe," *Proc. SPIE* **8442**(8442-26) (2012).

[3] Cropper, M. et al., "VIS: the visible imager for Euclid," *Proc. SPIE* **8442**(8442-99) (2012).

[4] Prieto, E. et al., "Euclid near-infrared spectrophotometer instrument concept at the end of the phase A study," *Proc. SPIE* **8442**(8442-10) (2012).

[5] Loose, M., Beletic, J., Garnett, J., and Xu, M., "High performance focal plane arrays based on the HAWAII-2RG/4RG and the SIDECAR ASIC," *Proc. SPIE* **6690** (2007).

[6] Cropper, M. et al., "Lessons learned from GAIA," *Euclid Consortium Meeting* (2015).

[7] Na-Nakornpanom, A., Naylor, B., and Lee, R. A., "In flight cryogenic behavior of the OCO-2 cryocooler," *IOP Conf. Series: Materials Science and Engineering* **101**, 012024–1–8 (June 2015).

[8] Rogalski, A., "HgCdTe infrared detector material: history, status and outlook," *Reports on Progress in Physics* **68**, 2267–2336 (2005).

[9] Li, H. H., "Refractive index of ZnS, ZnSe, and ZnTe and its wavelength and temperature derivatives," *J. Phys. Chem. Ref. Data* **13**(103-150) (1984).

[10] Elidrissi, B., Addou, M., Regragui, M., Bourgrine, A., Kachouane, A., and Bernede, J. C., "Structure, composition and optical properties of ZnS thin films prepared by spray pyrolysis," *Materials Chemistry and Physics* **68**, 175–179 (2001).

[11] IEST, "IEST-STD-CC1246D: Product cleanliness levels and contamination control program," (2002).

[12] Warren, S. G., "Optical constants of ice from ultraviolet to the microwave," *Appl. Opt.* **23**(8), 1206–1225 (1984).

[13] Warren, S. G., "Optical constants of carbon dioxide ice," *Appl. Opt.* **25**(16), 2650–2674 (1986).

[14] Dow Corning, "Safety data sheet dow corning(r) diffusion pump oil 704." www.dowcorning.com (October 2015).

[15] GmbH, W.-C., "Wacker silicon fluids," Online Brouchure, Hanns-Seidel-Platz 4, D-81737 München, Germany (2016).

[16] ESA, "Euclid spacecraft description," (March 2016).